Rainfall rate retrieval with IDRA, the polarimetric X-band radar at Cabauw, Netherlands

Tobias Otto and Herman W.J. Russchenberg
TU Delft Climate Institute, Department of Geoscience and Remote Sensing, Stevinweg 1, 2628CN Delft, Netherlands, t.otto@tudelft.nl, h.w.j.russchenberg@tudelft.nl
(Dated: 30 May 2012)


Tobias Otto

Abstract

In 2012, a polarimetric X-band weather radar will be installed in the city of Rotterdam in the frame of the INTERREG IVB NWE programme RAINGAIN[1]. The purpose of this radar is the measurement of rainfall rate with a high spatial and temporal resolution to allow the urban water management authorities to cope with extreme rainfall events and to help preventing flood damage.

In order to define an optimum rainfall rate retrieval algorithm for the Rotterdam radar, we evaluate in this contribution a rainfall rate retrieval algorithm based on differential phase measurements. For this study, we are using data acquired by the polarimetric X-band radar IDRA which is operated since 2007 at the Dutch national meteorological observatory CESAR[2].

1. Introduction

Weather radars are common to measure the spatial distribution and the temporal evolution of precipitation over a wide range. The operational weather radar network of Europe (EUMETNET/OPERA Radar Network) that covers the whole of Europe currently consists of 194 radars working at S- and C-band[3]. Those radars provide a low elevation precipitation scan with a spatial and temporal resolution down to 1x1 km² every 5 minute. This coarse resolution is a result of the sparse placement of these radars, and the volume scanning strategy that is required to accommodate the multitude of stakeholders such as weather fore- and now-casters, aviation meteorologists, and hydrologists.

In recent years, radar meteorologists exploit X-band weather radars for dedicated, short-range (<50 km) applications as:

- gap-filling radars in complex terrain such as mountainous areas, Météo France Dossier de Presse (2011),
- to obtain high-resolution rainfall data in densely populated urban areas for the improvement of urban water management and flood prediction, Maki et al. (2008), RAINGAIN project[1],
- to improve the low-altitude radar coverage, McLaughlin et al. (2009).

The compactness of X-band weather radars makes them easily deployable even in urban areas. Furthermore, they can provide a higher temporal and spatial resolution than standard operational weather radars because of the reduced range coverage, and the less stringent requirements on the scanning strategy due to their focused application.

However, the *X-band challenge* for the observation of precipitation is the significant higher level of attenuation by rain. Cloudbursts with instantaneous rainfall rates >100 mmh^{-1} may even lead to the total extinction of the radar signal within few kilometres. One way to counteract on the attenuation issue is the use of polarimetric radars at linear horizontal / vertical polarisation basis. Such radars can directly measure the differential phase, i.e. the phase difference between the co-polarised echoes at horizontal and vertical polarisation. The differential phase is a self-calibrating measurement, and, furthermore, it is not affected by attenuation unless the radar signal is totally extinct. However, because the scattering regime at X-band can be non-Rayleigh already in moderate rain, the differential phase is a superposition of the differential phase on propagation and on backward-scattering. In Otto and Russchenberg (2011), we proposed a method to estimate the range derivative of the differential propagation phase, the specific differential phase K_{dp}, and the differential backscatter phase δ_{co}. By reflectivity-weighting, this method also achieves an improved range resolution compared to conventional K_{dp} estimators. In this contribution we applied this method for the estimation of K_{dp} and in turn for the estimation of the rainfall rate. The polarimetric weather radar terminology and the scattering computation methodology are introduced in the next section followed by a detailed description of the rainfall rate estimation algorithm. Finally, the rainfall rate is estimated for an IDRA rain measurement in September 2011, and some conclusions are drawn.

2. Basics

Usual polarimetric weather radar observables include the reflectivities $Z_{hh,vv}^{att}$ based on the co-polarised echoes at horizontal (*hh*) and vertical (*vv*) polarisation, and the differential phase $\Psi_{dp}^{2\text{-way}}$:

$$Z_{hh,vv}^{att}(r_n) = Z_{hh,vv}(r_n) - 2\int_{r_1}^{r_{n-1}} \alpha_{hh,vv}^{1\text{-way}}(r)dr \quad (1)$$

[1] http://www.raingain.eu.
[2] CESAR – Cabauw Experimental Site for Atmospheric Research, http://www.cesar-observatory.nl.
[3] OPERA – Operational Programme for the Exchange of Weather Radar Information, “Radar database v1.17”, http://www.knmi.nl/opera, March 2012.

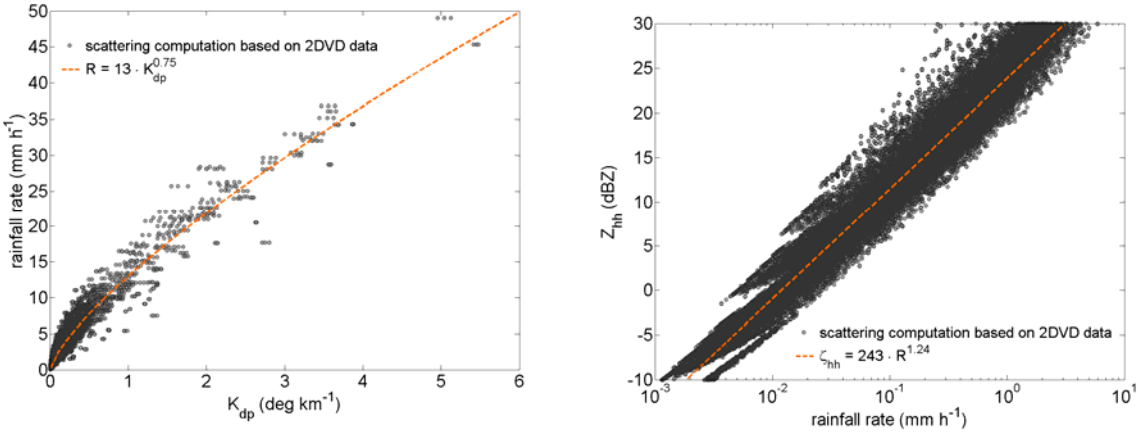

Fig. 1: Relationships used for the rainfall rate estimation at X-band based on scattering computations using 41530 RDSD's measured by a 2D video distrometer throughout the year 2009 at Cabauw and corresponding fits: (a) rainfall rate vs. K_{dp}, (b) Z_{hh} vs. rainfall rate for $Z_{hh} \leq 30$dBZ.

$$\Psi_{dp}^{2\text{-way}}(r_n) = \delta_{co}(r_n) - 2\int_{r_1}^{r_{n-1}} K_{dp}(r)dr \quad . \tag{2}$$

The first term in (1) and (2), i.e. the intrinsic reflectivities $Z_{hh,vv}$ and the differential backscatter phase δ_{co} stem from the backward-scattering in the range-bin r_n. The second terms consisting of the specific attenuations $\alpha_{hh,vv}^{1\text{-way}}$ and the one-way specific differential phase K_{dp} are due to the propagation of the radar signal from the radar at range r_1 to the leading edge of the range bin r_n. In case of rain, all terms in (1) and (2) can be related to the raindrop-size distribution (RDSD) $N(D)$:

$$\zeta_{hh,vv} = \frac{\lambda^4}{\pi^5 |K|^2} 10^{18} \int_D \sigma_{hh,vv}(D) N(D) dD \tag{3}$$

$$\alpha_{hh,vv}^{1\text{-way}} = 8.686 \cdot 10^3 \cdot \lambda \int_D \Im\left[f_{hh,vv}(D) \right] N(D) dD \tag{4}$$

$$\delta_{co} = \arg\left[\int_D s_{hh}^*(D) s_{vv}(D) N(D) dD \right] \tag{5}$$

$$K_{dp} = \frac{180}{\pi} 10^3 \cdot \lambda \int_D \Re\left[f_{hh}(D) - f_{vv}(D) \right] N(D) dD \, . \tag{6}$$

In (3) - (6), D is the equivolumetric raindrop diameter, λ is the wavelength, $|K|^2$ the dielectric factor, $\sigma_{hh,vv}=4\pi|s_{hh,vv}|^2$ are the radar cross sections at linear horizontal and linear vertical polarisation with $s_{hh,vv}$ and $f_{hh,vv}$ representing the backward- and the forward-scattering amplitudes of the hydrometeors, respectively. The reflectivity is usually displayed in logarithmic units

$$Z_{hh,vv}(\text{dBZ}) = 10 \log_{10}\left(\frac{\zeta_{hh,vv}}{1\text{mm}^6\text{m}^{-3}} \right). \tag{7}$$

For scattering computations, we obtain numerical values of the forward- and backward-scattering amplitudes for rain using the Fredholm integral method, Holt et al. (1978), with the model for the complex refractive index of water given by Liebe et al. (1991). Three oblate, spheroidal raindrop shape models were used: Brandes et al. (2005), Thurai et al. (2007), and a combination of Keenan et al. (2001) for D < 1.35 mm, Andsager et al. (1999) for 1.35 mm ≤ D ≤ 4.4 mm, and Beard and Chuang (1987) for D > 4.4 mm (KAB). To properly represent the natural variability of rain, we use 41530 RDSD's measured by a 2D video-disdrometer throughout the year 2009 at Cabauw, Leijnse et al. (2010). To include also variations of the raindrop temperature, the air temperature at 1.5 m height measured operationally at Cabauw was used.

The following section introduces an algorithm to invert of the radar measurements, specifically the reflectivity and the specific differential phase, in order to estimate the rainfall rate.

Rainfall rate estimation

The radar observables introduced in the previous section can be linked to the rainfall rate which in turn is given by

$$R = \frac{3.6}{10^3} \cdot \frac{\pi}{6} \cdot \int_D v(D) D^3 N(D) dD \tag{8}$$

with $v(D)$ the raindrop terminal velocity. Traditionally, only the reflectivity is used to estimate the rainfall rate because it was the only measurement that the first weather radars could obtain. However, the reflectivity is not the most favourable choice because it is prone to radar signal attenuation and to radar mis-calibration which might corrupt the rainfall rate estimates. A polarimetric weather radar measurement that is not affected by these issues is the differential phase, (2). At X-band in moderate to strong rain non-Rayleigh scattering may occur with the result that the differential phase is not only the range accumulation of the specific differential phase K_{dp}, (6), but it is superposed by the differential backscatter phase δ_{co},

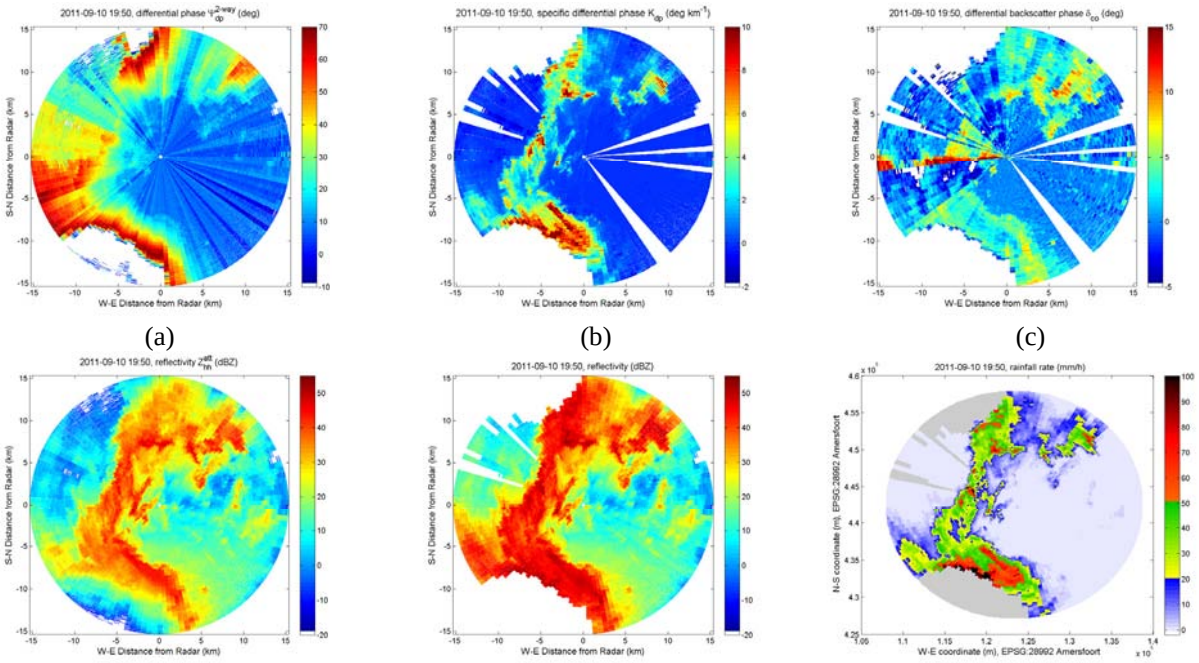

Fig. 2: For the IDRA measurement (2011-09-10 19:50UTC) plan position indicators are shown of (a) the measured differential phase $\Psi_{dp}^{2\text{-way}}$ (deg) which is decomposed into (b) the specific differential phase K_{dp} (deg km^{-1}) and (c) the differential backscatter phase δ_{co}. K_{dp} is used with (10) to correct (d) the measured reflectivity Z_{hh}^{att} (dBZ) for attenuation resulting in (e) Z_{hh} (dBZ). K_{dp} and Z_{hh} are used for the estimation of (f) the instantaneous rainfall rate (mm h^{-1}) as explained in the text. Note that (a)-(e) show the data in the radar-centred polar coordinate system (30 m range resolution) while for (f) the data is mapped to the RD New coordinates with a spatial resolution of 100x100 m. Grey-shaded areas in (f) show regions where the radar data is flagged as unavailable due to receiver saturation or total radar signal extinction.

(5). In such cases, methods like Hubbert and Bringi (1995), Otto and Russchenberg (2011) can be applied to separate K_{dp} and δ_{co}. Next we describe how K_{dp} is used in the context of quantitative precipitation estimation (QPE) for the TU Delft IRCTR drizzle radar (IDRA), Figueras i Ventura and Russchenberg (2009).

Before the rainfall rate estimation, the radar data undergoes pre-processing steps which for IDRA comprise spectral processing including a polarimetric spectral clutter suppression, Unal (2009), and estimation of the polarimetric weather radar observables as outlined by Figueras i Ventura (2009, Section 4.2.7). Range segments of receiver saturation and total radar signal extinction are detected and removed from further data processing. We then separate profile-by-profile the forward- and backward-scattering components of the reflectivity and the differential phase. First K_{dp} and δ_{co} are estimated, Otto and Russchenberg (2011), when the following condition is met

$$\max(\Psi_{dp}) - \min(\Psi_{dp})\Big|_{Z_{hh}^{att} > 25 dBZ} > 5\,\text{deg}\,. \tag{9}$$

K_{dp} is used to estimate the specific attenuation at horizontal polarisation, Holt (1988), applying the linear relation

$$\alpha_{hh}^{\text{1-way}} = 0.34 \cdot K_{dp} \tag{10}$$

with $\alpha_{hh}^{\text{1-way}}$ (dB km^{-1}) and K_{dp} (deg km^{-1}). This relation is valid for X-band (9.475 GHz) and has been determined by scattering computations as outlined in the previous section. In case that the differential phase accumulation for one profile does not exceed the threshold defined in (9), the attenuation is estimated by

$$\alpha_{hh}^{\text{1-way}} = 2.82 \times 10^{-5} \cdot 10^{Z_{hh}^{att}/10} \tag{11}$$

with $\alpha_{hh}^{\text{1-way}}$ (dB km^{-1}) and Z_{hh}^{att} (dBZ). Also this relation is valid for X-band (9.475 GHz) and has been determined by scattering computations taking only reflectivities equal to or less than 30 dBZ into account. We also account for gaseous attenuation applying (3.19) from Doviak and Zrnić (1993).

For the estimation of the rainfall rate R the following relations are applied

$$R = 13 \cdot K_{dp}^{0.75} \tag{12}$$

$$\zeta_{hh} = 243 \cdot R^{1.24} \text{ valid for } Z_{hh} \le 30 \text{ dBZ} \tag{13}$$

with R (mm h^{-1}), K_{dp} (deg km^{-1}) and ζ_{hh} (mm^6 m^{-3}). The result of the scattering computations that have been used to determine (12) and (13) are displayed in Fig. 1. The raindrop terminal fall velocity relation given by Atlas et al. (1973) has been employed. Note that (13) is only valid for reflectivities equal to or less than 30 dBZ. Finally, for the estimation of the

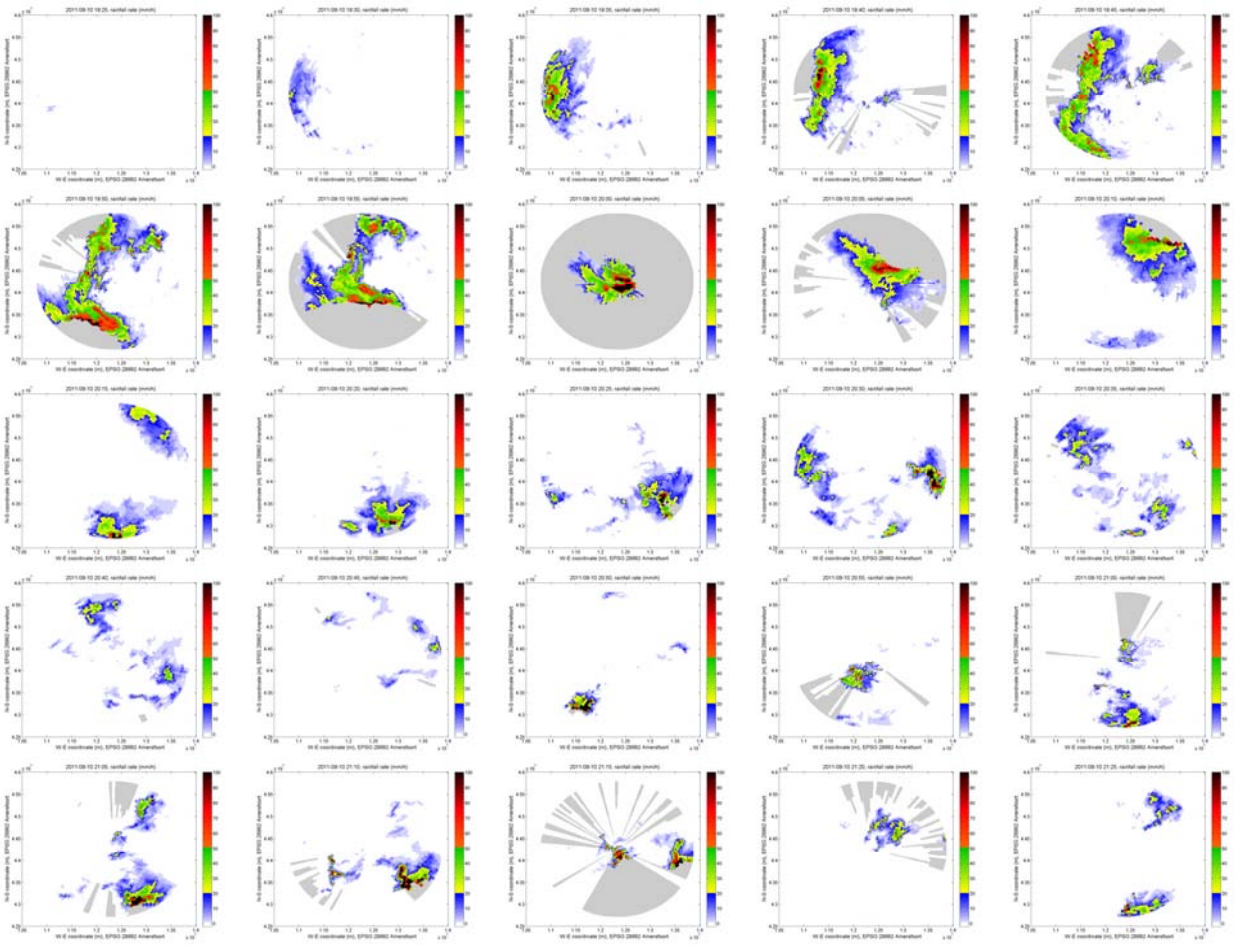

Fig. 3: Temporal evolution of the case study showing the IDRA rainfall rate estimate every 5 minutes. Note that IDRA is constantly rotating at a fixed low elevation angle, providing an update of the rainfall rate once per minute.

rainfall rate, (12) is used whenever K_{dp} is available, its standard deviation is less than 2 deg km^{-1} and Z_{hh} > 30 dBZ, else (13) is used.

As a last step, the rainfall rate is mapped from the radar-centred polar coordinate system to the Dutch Rijksdriehoekscoördinaten EPSG 28992 Amersfoort (RD New) with a spatial resolution of usually 100x100 m and a temporal resolution of 1 minute.

Heavy rain case study 2011-09-10

To test the rainfall rate retrieval as outlined in the previous section, we applied the method to IDRA data from 2011-09-10 19:00-21:30UTC where IDRA measured heavy precipitation as a result of a cold front passing over the Netherlands. The polarimetric X-band radar IDRA (1 round per minute) is placed on top of the 213 m high meteorological tower at CESAR, Fig. 4(a), and is scanning continuously with 1 round per minute at a fixed low elevation angle of 0.5 deg. For this measurement, IDRA which is a frequency-modulated continuous wave radar was set to its standard mode with a sweep time of 409.6 µs and a frequency excursion of 5Mhz which results in 512 range bins with a range resolution of 30 m, i.e. 15.36 km maximum range.

Fig. 2 shows plan position indicators of the IDRA measurement at 19:50UTC, specifically, Fig. 2(a) shows the measured differential phase $\Psi_{dp}^{2\text{-way}}$ (deg) which is decomposed into Fig. 2(b) the specific differential phase K_{dp} (deg km^{-1}) and Fig. 2(c) the differential backscatter phase δ_{co}. K_{dp} is used with (10) to correct Fig. 2(d) the measured reflectivity Z_{hh}^{att} (dBZ) for attenuation resulting in Fig. 2(e) Z_{hh} (dBZ). K_{dp} and Z_{hh} are then used for the estimation of Fig. 2 (f) the instantaneous rainfall rate (mm h^{-1}) as explained in previous section. Note that Fig. 2(a)-(e) show the data in the radar-centred polar coordinate system (30 m range resolution) while for Fig. 2(f) the data is mapped to the RD New coordinates with a spatial resolution of 100x100 m. Grey-shaded areas in Fig. 2(f) show regions where the radar data is flagged as unavailable due to receiver saturation or total radar signal extinction. Fig. 2(b) shows that due to the strength of this precipitation event, K_{dp} is almost everywhere available. Note also the high spatial resolution of K_{dp} compared to conventional estimators which is achieved by reflectivity-weighting based on the self-consistency principle, Otto and Russchenberg (2011). The high spatial resolution of K_{dp} translates directly into a high spatial resolution of the rainfall rate estimate.

Fig. 3 shows the rainfall rate estimates for this event in time steps of five minutes. However, note that not all data is shown due to space constraints; IDRA is providing a higher temporal resolution of one minute. From Fig. 3 (20:00UTC) it is evident that attenuation poses a major limitation in heavy precipitation for an effective rainfall rate estimation over larger

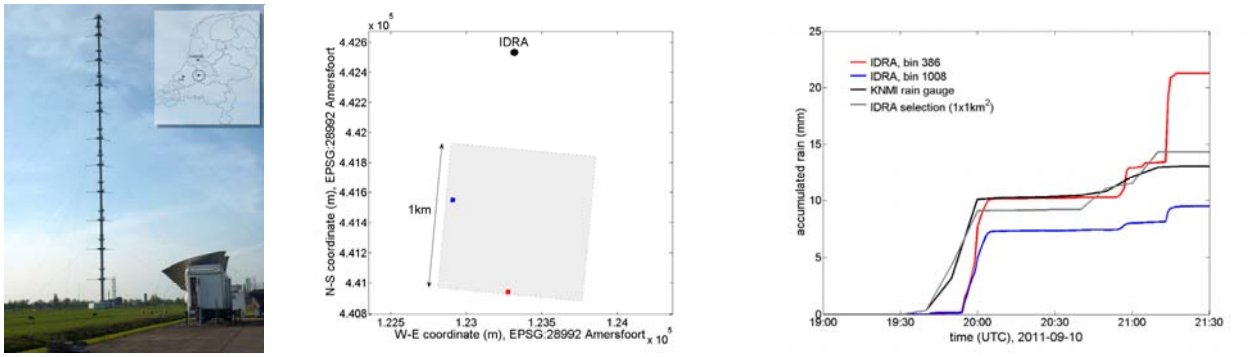

(a) (b) (c)

Fig. 4: (a) Photo of the two TU Delft radar (profiling S-band radar TARA, and scanning X-band radar IDRA on top of the tower) at CESAR, (b) selection of a 1x1 km² area 500 m south of IDRA divided into a grid of 30x30 m, and (c) accumulated rain for the case study 2011-09-10 measured by IDRA and the KNMI rain gauge.

areas at X-band. Therefore, instead of a stand-alone installation of an X-band weather radar for QPE, a network of X-band radars should be favoured, or the X-band measurements need to be complemented in heavy precipitation with data from the operational weather radar network.

To fully exploit the high-spatial resolution of IDRA, we mapped the rainfall rate within the 1x1km² area south of IDRA shown in Fig. 4(b) onto a grid of 30x30 m resolution. For the selected case study, Fig. 4(c) shows the rain accumulation for:

- the KNMI rain gauge which is placed close to IDRA (black curve),
- the IDRA rainfall rate estimate averaged in space over the 1x1km² shown in Fig. 4(b) and in time to match the temporal resolution (10 minutes) of the KNMI rain gauge (grey curve),
- the IDRA rainfall rate for the blue 30x30 m grid point highlighted in Fig. 4(b) (blue curve),
- the IDRA rainfall rate for the red 30x30 m grid point highlighted in Fig. 4(b) (red curve).

From Fig. 4(c) it can be seen that the in space and time averaged IDRA rainfall rate estimate (grey curve) fits very well with the KNMI rain gauge measurement (black curve) although the rain gauge is placed close to IDRA and not within the 1x1 km² area shown in Fig. 4(b). The difference of rain accumulation at 21:30UTC is only about 1.3 mm which provides confidence in the rainfall rate estimation outlined in the previous section, this good match between IDRA and the rain gauge was also confirmed for other rainfall events by Bruni et al. (2012).

The red and the blue curve in Fig. 4(c) show the rain accumulation from the 30x30 m grid points highlighted in Fig. 4(b). Although the grid points are only about 700 m apart, the rain accumulation at 21:30UTC differs by 11.8 mm. One of the reasons for this is certainly the high spatial and temporal variability of this event, Fig. 3. It therefore suggests the need for high-resolution radar observations both in space and time especially for hydrological applications in urban water management and flood prediction in cities at street scale. Also, due to the temporal variability, a strong precipitation core might not be sampled at a specific location because of the low revisit time of IDRA of one minute. Thus, it might be beneficial to link the rainfall rate estimation to a storm-tracking algorithm or to setup adaptive scanning strategies for such dynamic precipitation events.

Conclusions

In this contribution, we presented a rainfall rate estimation algorithm for IDRA, the scanning, polarimetric X-band radar at CESAR. The algorithm is based on a high spatial resolution estimate of the specific differential phase whenever it is available to avoid issues such as radar calibration or attenuation. The algorithm is not final yet; it misses a hydrometeor classification and a melting layer height detection. However, most of the time, IDRA is measuring in rain due to the low elevation angle, the limited range of 15 km in the standard mode and the moderate temperatures in the Netherlands.

We applied the algorithm successfully to a heavy rain case study in September 2011. The accumulated rain over a period of 2.5h averaged in space and time of IDRA matches well a co-located rain gauge measurement. However, further validation is required. For this event, a high spatial and temporal variability was observed which confirms the demand for high-resolution precipitation measurements, e.g. by X-band radars for dedicated purposes such as the rainfall rate estimation at street scale in urban environments for flood prediction and as an input to urban drainage models. To further improve high-resolution QPE, adaptive scanning strategies and rainfall rate estimation linked to storm-tracking algorithms should be investigated.

Later this year we will start to process all IDRA data collected so far with this algorithm, and to make the estimated rainfall rate freely available online at *http://www.cesar-database.nl* and *http://data.3tu.nl/repository/collection:cabauw*.

Acknowledgment

This study was supported by the INTERREG IVB NWE project RAINGAIN. The authors acknowledge the KNMI for providing the meteorological surface data at CESAR (available online at http://www.cesar-database.nl). We also thank Fred van der Zwan and Paul Hakkart for their technical support in operating IDRA.

References

Andsager K., Beard K.V., Laird N.F., 1999: Laboratory Measurements of Axis Ratios for Large Raindrops, *J. Atmos. Sci.*, **56**, 2673-2683.

Atlas D., Srivastava R.C., Sekhon R.S., 1973: Doppler Radar Characteristics of Precipitation at Vertical Incidence, *Rev. Geophys.*, **11**, 1-35.

Beard K.V., Chuang C., 1987: A New Model for the Equilibrium Shape of Raindrops, *J. Atmos. Sci.*, **44**, 1509-1524.

Brandes E.A., Zhang G., Vivekanandan J., 2005: Corrigendum, *J. Appl. Meteor.*, **44**, 186.

Bruni G., ten Veldhuis J.A.E., Otto T., Leijnse H., 2012: Rainfall resolution from weather radars and their application in urban drainage modelling, *Geophysical Research Abstracts*, **14**, EGU General Assembly 2012, EGU2012-3317.

Doviak R.J., Zrnić D.S., 1993: Doppler Radar and Weather Observations, 2nd edition, *Academic Press*.

Figueras i Ventura J., Russchenberg H. W. J., 2009: Towards a better understanding of the impact of anthropogenic aerosols in the hydrological cycle: IDRA, IRCTR drizzle radar. *Phys. Chem. Earth, Parts A/B/C*, **34**, 88 – 92.

Figueras i Ventura J., 2009: Design of a High Resolution X-band Doppler Polarimetric Radar, *PhD thesis*, TU Delft, available online at http://repository.tudelft.nl/view/ir/uuid%3Ad90b9ad6-237b-435d-9dc5-5660d9e7fbdd/.

Holt A.R., Uzunoglu N.K., Evans B.G., 1978: An integral equation solution to the scattering of electromagnetic radiation by dielectric spheroids and ellipsoids, *IEEE Trans. Antennas Propag.*, **AP-26**, 706-712.

Holt A.R., 1988: Extraction of differential propagation phase from data from S-band circularly polarised radar, *Electron. Lett.*, **24**, 1241-1244.

Hubbert J., Bringi V.N., 1995: An Iterative Filtering Technique for the Analysis of Copolar Differential Phase and Dual-Frequency Radar Measurements, *J. Atmos. Oceanic Technol.*, **12**, 643-648.

Keenan T.D., Carey L.D., Zrnić D.S., May P.T., 2001: Sensitivity of 5-cm Wavelength Polarimetric Radar Variables to Raindrop Axial Ratio and Drop Size Distribution, *J. Appl. Meteor.*, **40**, 526-545.

Leijnse H., co-authors, 2010: Precipitation Measurement at CESAR, the Netherlands, *J. Hydrol.*, **11**, 1322-1329.

Liebe H.J., Hufford G.A., Manabe T., 1991: A model for the complex permittivity of water at frequencies below 1 THz, *Int. J. Infrared Millim. Waves*, **12**, 659-675.

Maki M., co-authors, 2008: X-band Polarimetric Radar Network in the Tokyo Metropolitan Area: X-NET, *Proceedings of ERAD2008, The Fifth European Conference on Radar in Meteorology and Hydrology*.

McLaughlin D., co-authors, 2009: Short-wavelength technology and the potential for distributed networks of small radar systems, *B. Am. Meteorol. Soc.*, **90**, 1797-1817.

Météo France Dossier de Presse, 2011: Présentation du premier radar du réseau RHyTMME.

Otto T., Russchenberg H.W.J., 2011: Estimation of Specific Differential Phase and Differential Backscatter Phase from polarimetric Weather Radar Measurements of Rain, *IEEE Geosci. Remote Sens. Lett.*, **8**, 988-992.

Thurai M., Huang G.J., Bringi V.N., Randeu W.L., Schönhuber M., 2007: Drop Shapes, Model Comparisons, and Calculations of Polarimetric Radar Parameters in Rain, *J. Atmos. Oceanic Technol.*, **24**, 1019-1032.

Unal C., 2009: Spectral Polarimetric Radar Clutter Suppression to Enhance Atmospheric Echoes, *J. Atmos. Oceanic Technol.*, **26**, 1781-1797.